Supplementary Information (SI) for New Journal of Chemistry.
This journal is © The Royal Society of Chemistry and the Centre National de la Recherche Scientifique 2024

Br-triggered $BiVO_4$ photoanode surface for efficient solar water splitting

Yuhong Wang[a,*], Qingqing Cheng[a], Weijie Cheng[a], Shaoqing Guo[a,*], Honghong Zhao[b,*], Lizhen Gao[c,d]

[a]School of Environment and Resource, Taiyuan University of Science and Technology, Taiyuan 030024, P. R. China.

E-mail: wangyuhong@tyust.edu.cn

E-mail: guosq@tyust.edu.cn

[b]School of Materials Science and Engineering, North University of China, Taiyuan 030051, PR China

E-mail: honghongzhao@nuc.edu.cn

[c]College of Environmental Science and Engineering, Taiyuan University of Technology, Taiyuan 030024, P. R. China.

[d]School of Mechanical Engineering, University of Western Australia, 35 Stirling Highway, WA 6009, Australia.

Equations used in this work[1]:

1. Calculation of applied bias photon-to-current efficiency (ABPE):

$$ABPE = \frac{J_{PEC} \times (1.23 - V_{app})}{P_{light}} \qquad (S1)$$

J_{PEC} (mA·cm^{-2}) is the measured photocurrent density; V_{app} (V) is the applied external potential vs. RHE and P_{light} (100mW·cm^{-2}) is the power density of the illumination.

2. Calculation of incident-photon-to-current conversion efficiency (IPCE):

$$IPCE = \frac{J_{\lambda} \times 1240}{\lambda \times P_{\lambda}} \qquad (S2)$$

J_{λ} (mA·cm^{-2}) is the photocurrent density measured under monochromatic illumination at λ; P_{λ} (mW·cm^{-2}) is the power intensity of the incident monochromatic light at wavelength λ; the value of 1240 (V.nm) is calculated from the equation of hc/e, where e is the charges of one electron (1.6 × 10^{-19} C); h is Planck's constant (6.63 × 10^{-34}J·s) and c is the speed of light (3 × 10^{8} m·s^{-1}).

3. Calculation of surface charges transfer efficiency (η_{CTE}):

$$\eta_{CTE} = \frac{J_{PEC}}{J_{scavenger}} \qquad (S3)$$

$J_{scavenger}$ (mA·cm^{-2}) and J_{PEC} (mA·cm^{-2}) are the measured photocurrent density in a 0.01 M sodium borate buffer solution (pH = 7.4) with and without 0.5 M Na_2SO_3.

4. Calculation of charges separation efficiency (η_{CSE}):

$$\eta_{CSE} = \frac{J_{scavenger}}{J_{abs}} \qquad (S4)$$

$J_{scavenger}$ is the measured photocurrent density in a 0.01 M sodium borate buffer solution (pH = 7.4) with 0.5 M Na_2SO_3 as a holessss scavenger.

5. The charges-transfer time (τ) of the films was calculated according to the equation[2]:

$$\tau = 1/2\pi f \qquad (S5)$$

where *f* is the minimum frequency of the imaginary components

Calculation detail:

The calculations were conducted within the framework of DFT as implemented in the plane wave set Vienna ab initio Simulation Package (VASP) code[3].The generalized gradient approximation with the Perdew–Burke–Ernzerhof functional was employed to describe the exchange–correlation interaction[4]. In all calculations, the van der Waals interaction was described by using the empirical correction in Grimme's scheme, i.e., DFT+D3[5]. The cutoff energy of the plane wave basis set was 500 eV. The geometries were optimized until the energy and the force were converged to 10^{-6} eV and 0.001 eV $Å^{-1}$, respectively. All calculations were spin polarized throughout the calculations. The Brillouin zone was sampled by gamma point.

The overall OER could be written as

$$2H_2O \rightarrow O_2 + 4H^+ + 4e^- \qquad (S6)$$

In our model, we assumed that the OER is processed in the four electrons pathway

$$H_2O(/) + {}^* \rightarrow OH^* + e^- + H^+ \quad (S7)$$
$$OH^* \rightarrow O^* + e^- + H^+ \quad (S8)$$
$$H_2O(/) + O^* \rightarrow OOH^* + e^- + H^+ \quad (S9)$$
$$OOH^* \rightarrow O_2(g) + e^- + H^+ \quad (S10)$$

where * refers to an active site on the catalyst, (l) and (g) represent liquid and gas phases, respectively. O*, HO*, and HOO* are adsorbed intermediates.For each step the reaction free energy (ΔG) was defined as the difference between free energies of the initial and final states and was given by the expression[6]

$$\Delta C = \Delta E + \Delta ZPE - T\Delta S + \Delta G_U + \Delta G_{ph} (S11)$$

where ΔE, ΔZPE, and ΔS were the different energy, zero-point energy, and entropy of the reaction, respectively. The ΔE was obtained from DFT calculation, while the ΔZPE and ΔS were calculated from the values of Table 1 in a previous report[7].The GH+ was defined as 1/2GH2 as suggested in the literature[7].ΔGU = −eU, in which U is the potential related to the standard hydrogen electrode. ΔGpH is the correction free energy of OH^-ions depended by the concentration (ΔGpH = −kT ln 10 × pH).

The minimum potential for OER was obtained by

$$U(OER) = max\{\Delta G_{1a}, \Delta G_{1b}, \Delta G_{1c}, \Delta G_{1d}\} (S12)$$

$$\eta_{OER} = \frac{U(OER)}{e} - 1.23 \quad (S13)$$

in which, ΔG1a, ΔG1b, and ΔG1c are the reaction free energy of Equations (S7)–(S10), when U = 0 V, pH = 0. ηOER (V) refers to the overpotential required for OER.

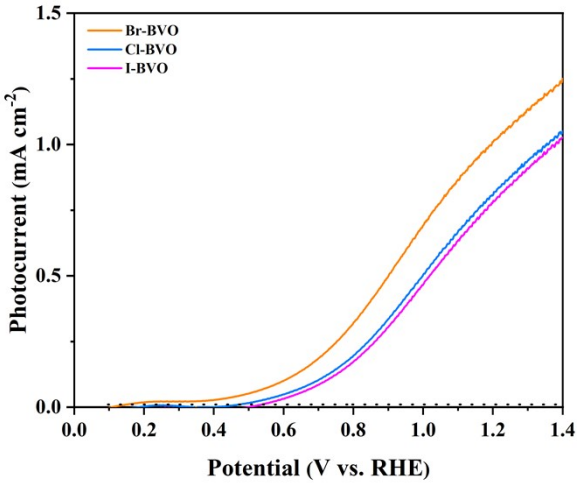

Figure S1 LSV Curves of photoelectrochemical spitting water of BVO photoanodes obtained at 0.5 M KBr/I/Cl for 2 h.

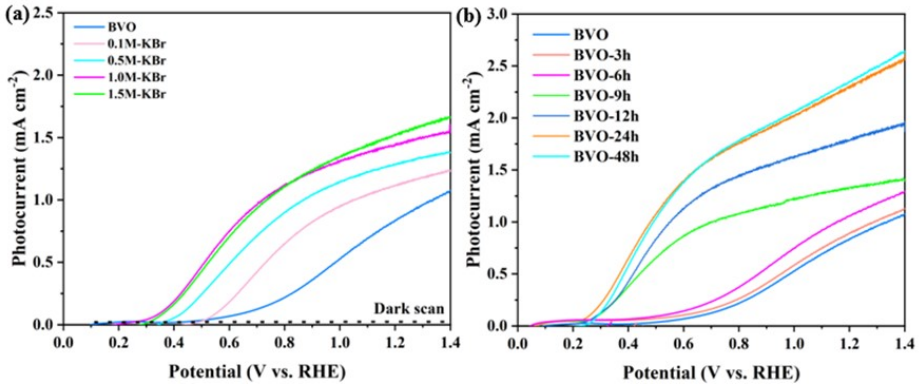

Figure S2 LSV curves of photoelectrochemical spitting water of BVO photoanodes obtained at (a) different concentration of KBr and (b) different post-treatment time

The optimal experimental conditions were described as follows: Firstly, the BVO photoanode was modified in 0.5 M KBr, KI and KCl solutions for the same time (2 h) at room temperature. The linear sweep voltammetry (LSV) curves of photoelectrochemical (PEC) water splitting indicated that the BVO photoanode modified by KBr solution had significant PEC perfomence (**Fig. S1**). Then, the BVO photoanode was modified for the same time (30 min) in different concentrations of KBr

solution. The modification effect on the BVO photoanode significantly increased with the rise of KBr concentration from 0.1 M to 1 M, as indicated by the LSV curves. However, the effect of 1 M and 1.5 M KBr on the BVO photoanode was similar (**Fig. S2a**). Therefore, the 1 M KBr solution had the optimal modification effect on the BVO photoanode. In addition, the BVO photoanode was post-treatment in 1 M KBr solution for different times (3,6,9,12,24,48 h) to study the effect of modification time on the PEC performance of BVO photoanode (**Fig. S2b**). With the increase of post-treatment modification time (3~24 h), the photocurrent of PEC water splitting gradually increased in the BVO photoanode. Nevertheless, the LSV curves of PEC water splitting were similar after post-treatment for 24 h and 48 h. Thus, the optimal post-treatment time was 24 h. The above trend of photocurrent change may be due to the fact that with the increase of post-treatment time, the coverage of the modified material on the surface of the BVO photoanode gradually increased, which induced a higher PEC water splitting photocurrent. After post-treatment for 24 h, the surface of the BVO photoanode was completely covered by the modified material. Although the subsequent modification time increased to 48 h, the coverage of the modified material on the surface of the BVO photoanode did not change, thus showing a similar LSV curve. Therefore, the optimal post-treatment condition of BVO photoanode is post-treatment for 24 h in 1 M KBr solution at room temperature.

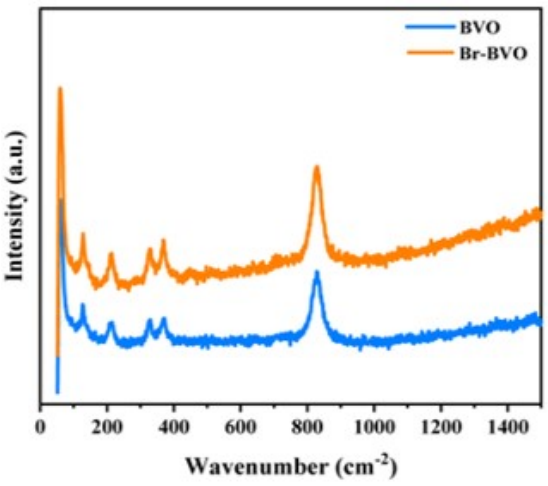

Figure S3 Raman spectras of BVO and Br-BVO photoanode

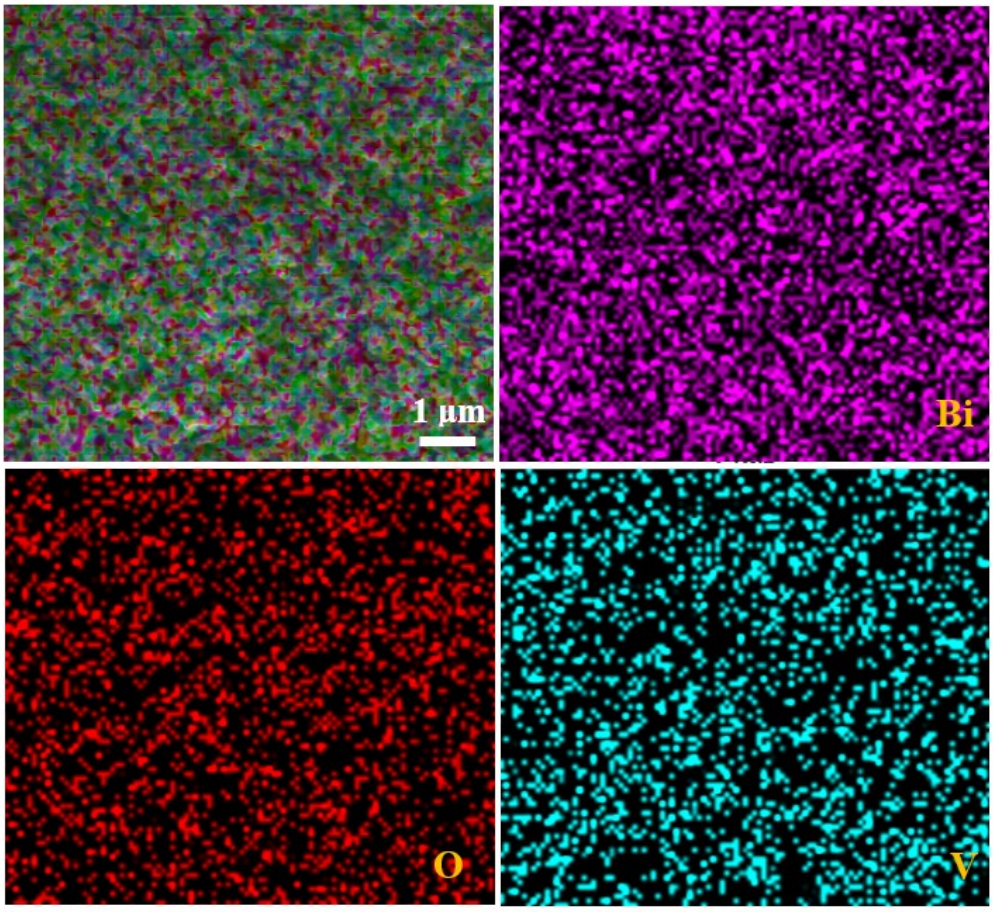

Figure S4 SEM energy-dispersive X-ray spectra (EDS) spectra elemental mapping of $BiVO_4$ photoanode.

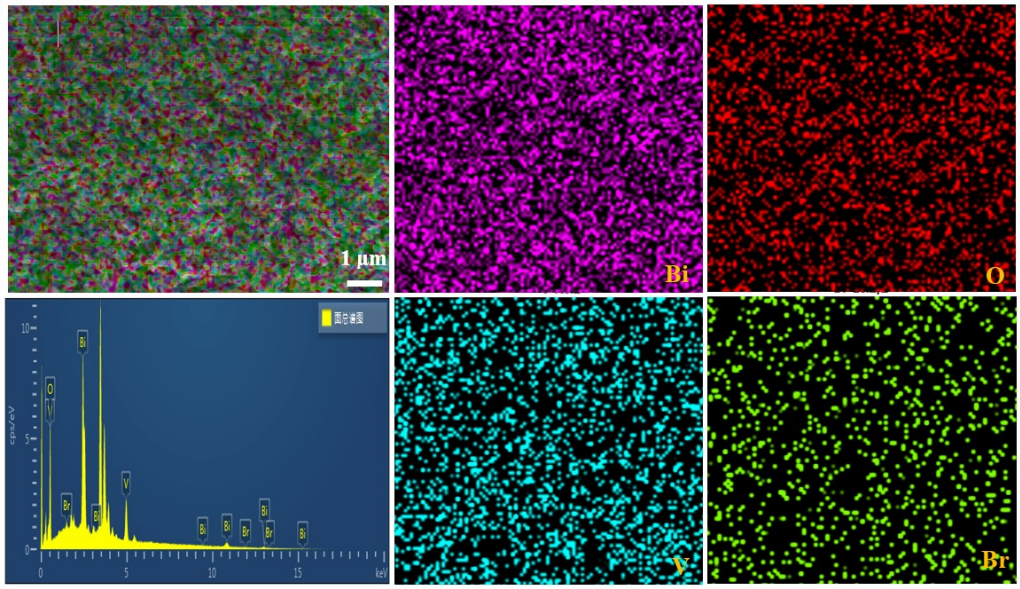

Figure S5 SEM energy-dispersive X-ray spectra (EDS) spectra elemental mapping of Br-$BiVO_4$ photoanode.

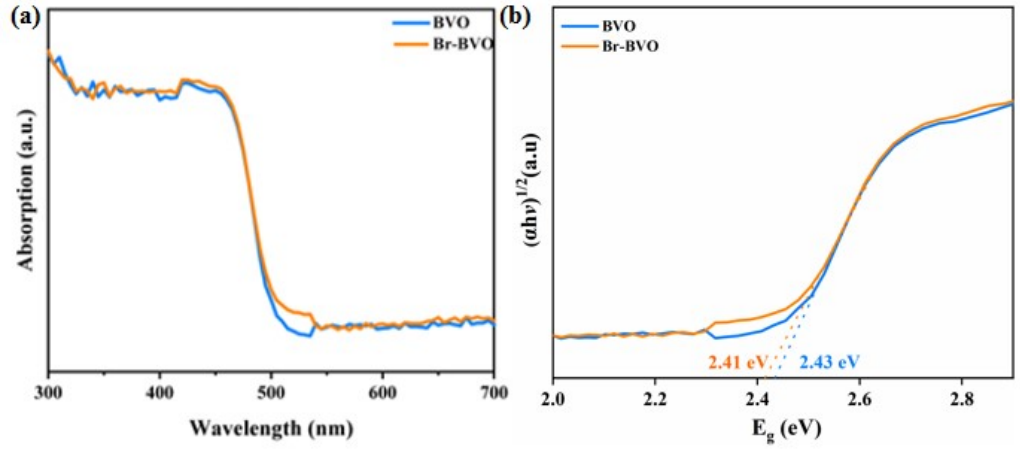

Figure S6 (a) UV-vis absorbance spectras and (b) Tauc plots of BVO and Br-BVO photoanode.

The band gap of the samples can be determined using the following formula[8]:

$$\alpha h\nu = A(h\nu - E_g)^{n/2} \qquad (S14)$$

Where α, h, ν, A, E_g and n are the absorption coefficient, Planck's constant, incident light frequency, proportionality constant, band-gap and the characteristic integer, respectively. Among them, n depends on the characteristics of the optical transition in

a semiconductor, i.e., direct transition (n=1) or indirect transition (n= 4). $BiVO_4$ pertains to indirect transition and the value of n is 4. The band-gap energy (E_g) of $BiVO_4$ can thus be estimated from a plot of $(\alpha hv)^2$ versus photon energy (hv). However, C_xN_y pertains to direct transition and the value of n is 1. The band-gap energy (E_g) of C_xN_y can thus be estimated from a plot of $(\alpha hv)^{1/2}$ versus photon energy (hv).

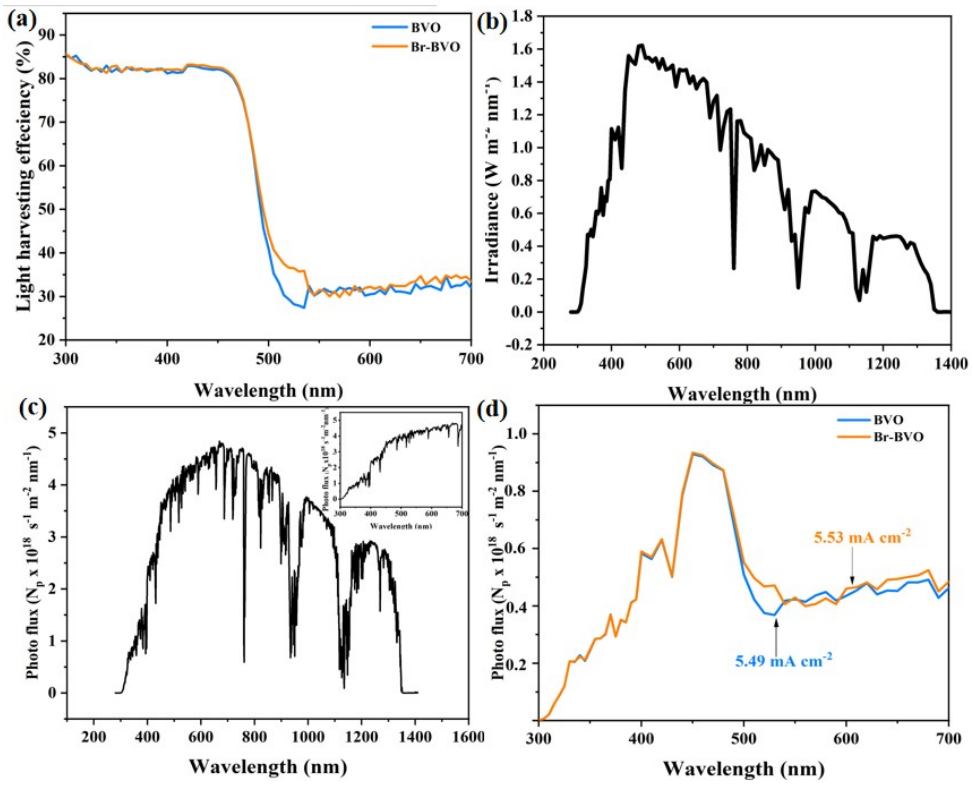

Figure. S7a: The light harvesting efficiency (LHE) of BVO and Br-BVO photoanode. It can be calculated by the absorbance data η_{ABS} shown in Figure S6a: $\eta_{LHE} = (1\text{-}10^{-\eta ABS}) \times 100\%$;

Figure. S7b: the solar spectral irradiance (original data of AM1.5G spectrum, named as (original data of AM 1.5G spectrum, named as "E");

Figure. S7c: the photo flux (the number of photons, N_p) which is converted from the irradiance data (Figure S7b): $Np=E/Ep=E\bullet[(\lambda\bullet10^{-9})/(h\bullet c)] = E\bullet\lambda\bullet10^{-9}/(1.988\bullet10^{-25})$ $=E\bullet\lambda\bullet5.03\bullet10^{15}$;

Figure. S7d: The charges density data (J_{abs})[9]. It can be obtained from the product of the photon flux Np (Figure S7c) ×e× light harvesting efficiency (Figure S7a); Where the e is the electric charges carried by a single electron (1.6022×10^{-19}); the $J_{max}\times\eta_{LHE}$ is the integration of the the photo flux by wavelength (nm). The J_{abs} $=J_{max}\times\eta_{LHE}$ of BVO and Br-BVO photoanode was integrated to be 5.49 mA/cm^2 and 5.53 mA/cm^2, respectively.

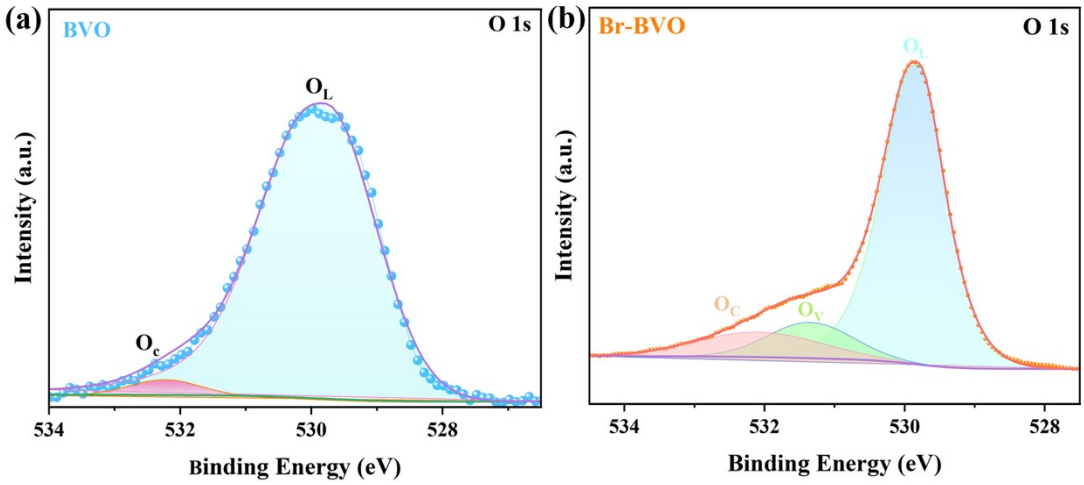

Figure S8 the O 1s spectra of (a) BVO and (b) Br-BVO phoaoanode.

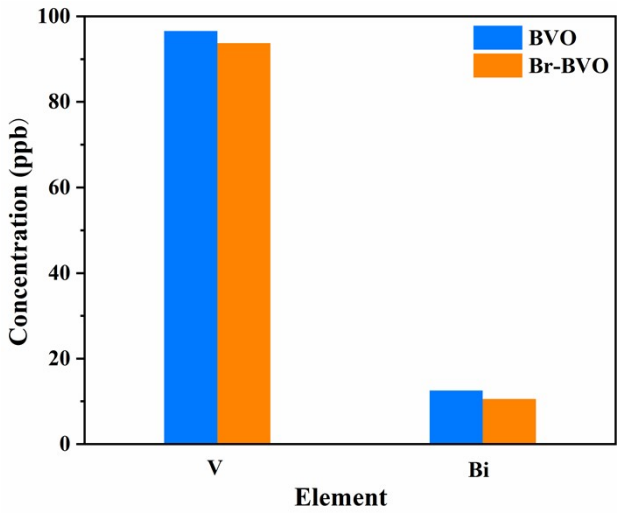

Figure S9 ICP analysis after stability test of BVO and Br-BVO photoanode.

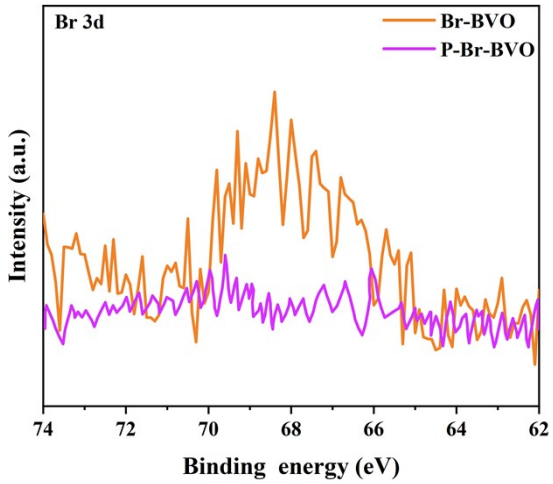

Figure S10 Comparison of XPS results of Br-BVO photoanode before and after.

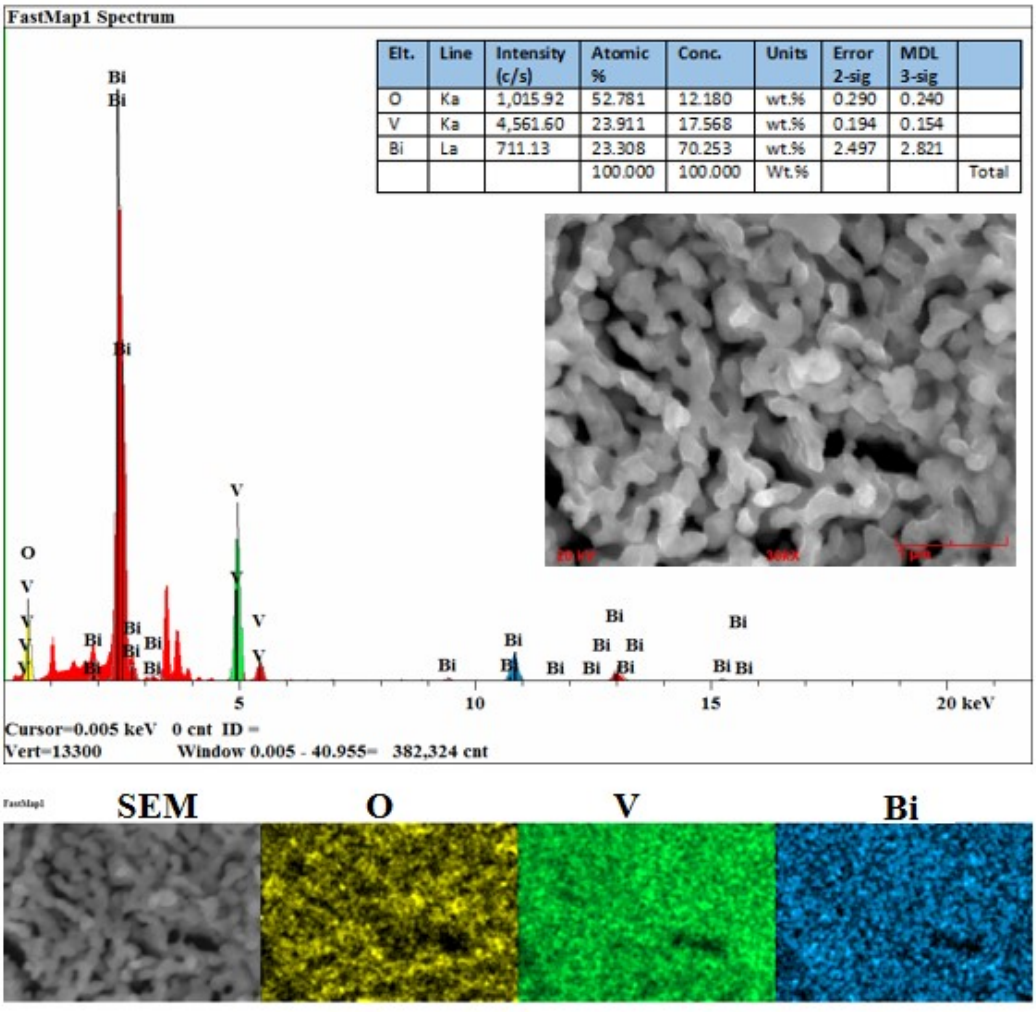

Figure.S11 the EDS-mapping after stability test.

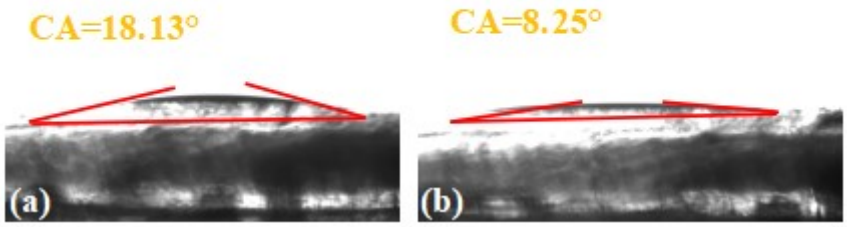

Figure S12 The contact angle tests of the BVO (a) and Br-BVO(b) photoanode.

The calculation of the work function (Φ) of $BiVO_4$ and Br-$BiVO_4$ according to their UV-vis and UPS spectra[10].

$BiVO_4$:

E_{Cutoff}=17.6 eV

Φ ($BiVO_4$) = hν-E_{Cutoff}= 21.22 eV-17.6 eV=3.62 Ev(S15)

Br-$BiVO_4$:

E_{Cutoff}=18.1 eV

Φ (Br-$BiVO_4$) = hν-E_{Cutoff}= 21.22 eV-18.1 eV=3.12 Ev(S16)

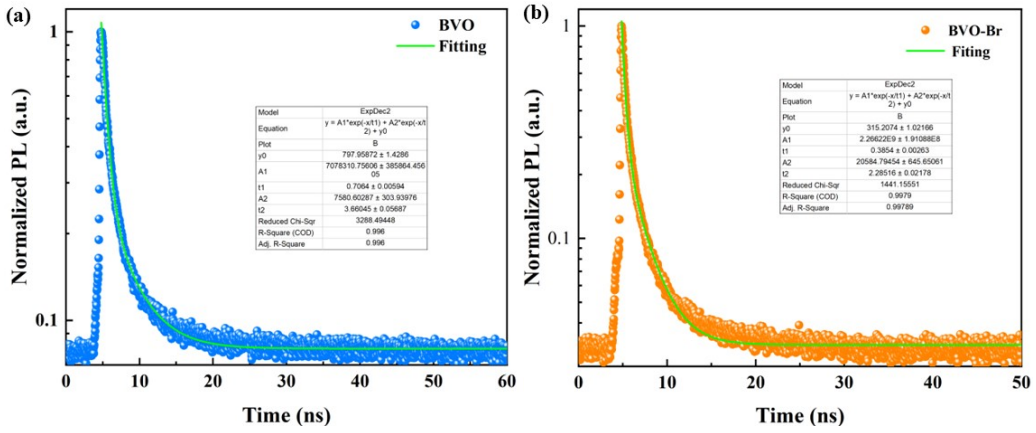

Figure S13 (a) TRPL measurements fitting plot of BVO and Br-BVO photoanode.

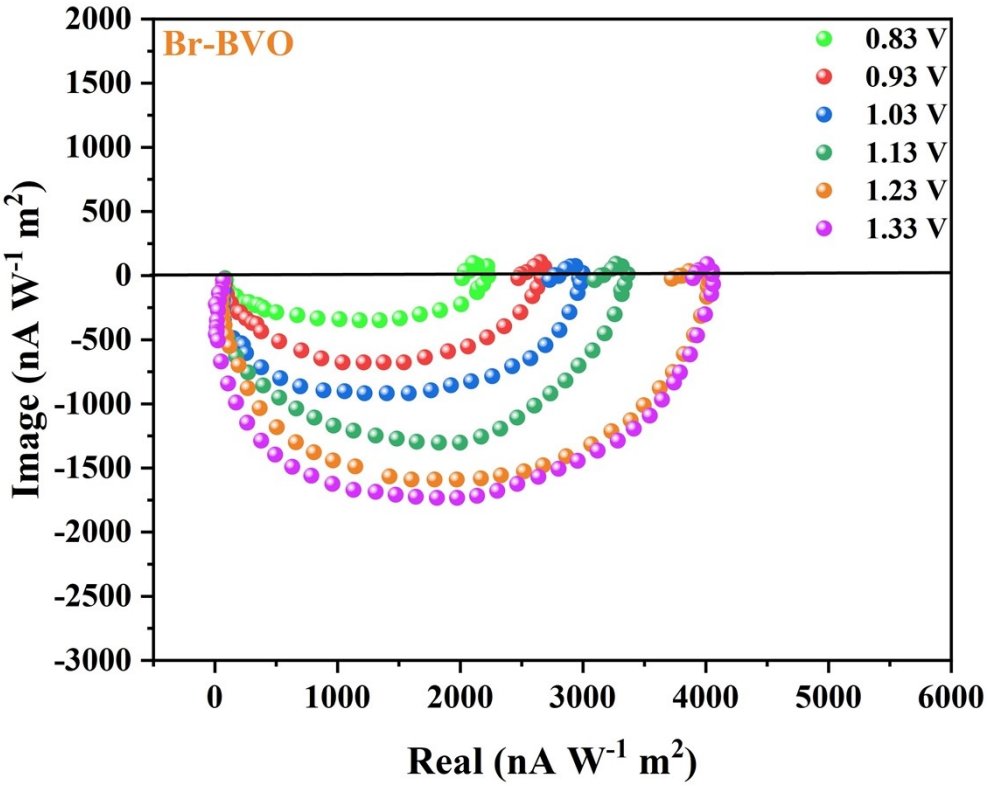

Figure S14 The IMPS Nyquist plots of Br-BVO photoanode recorded at different potentials (0.83 V_{RHE}-1.33 V_{RHE}).

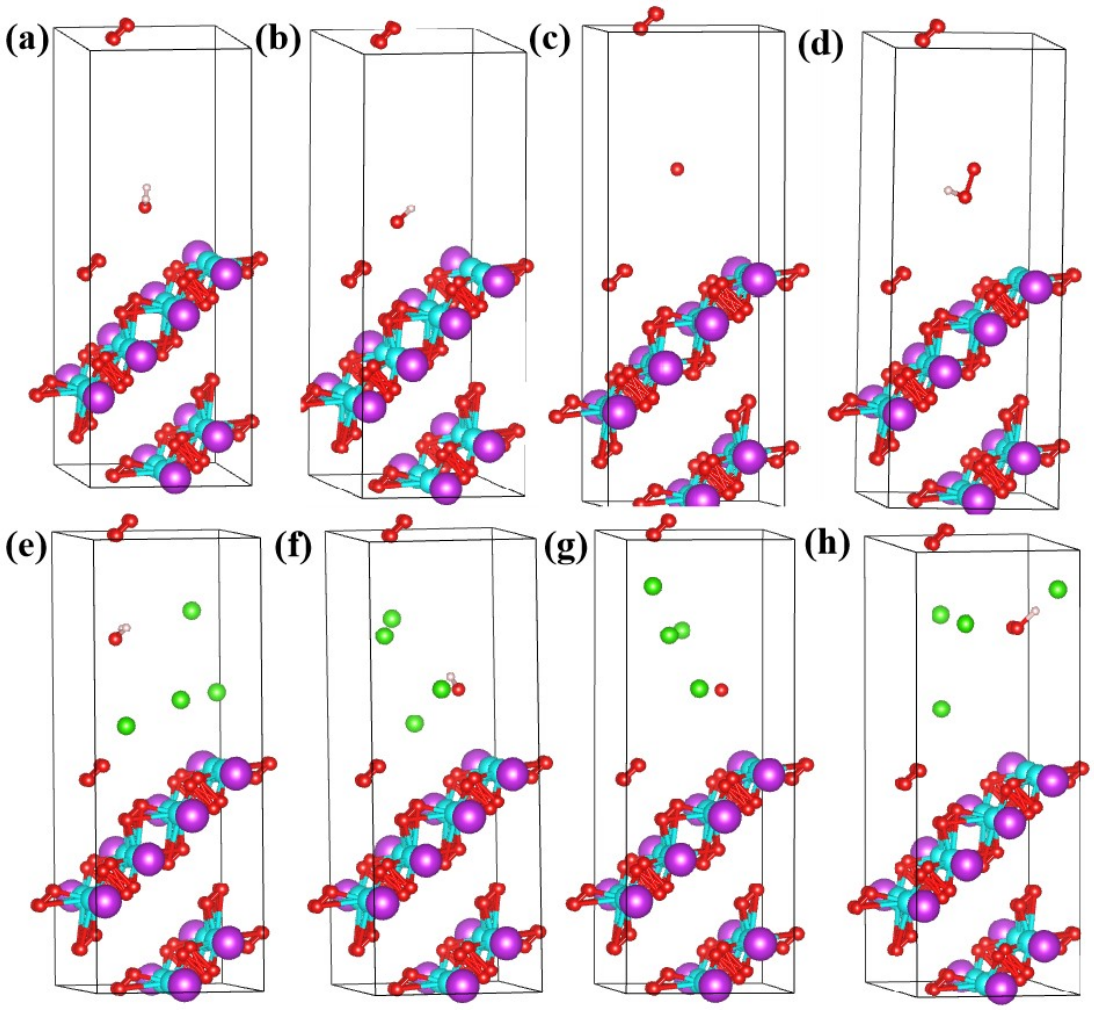

Figure S15 Adsorption model of (a) H_2O, (b) OH, (c) O and (d) OOH on BVO photoanode; adsorption model of (e) H_2O, (f) OH, (g) O and (h) OOH on Br-BVO photoanode.

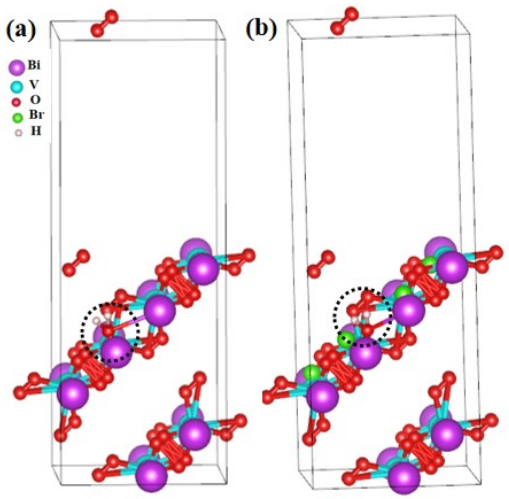

Figure S16 The initial DFT calculated adsorption model of the reactant H_2O on BVO and Br-BVO photoanode.

Table S1 The PEC performance of $BiVO_4$-based photoanodes without oxygen evolution.

Material	the power intensity of the incident light (mW/cm^2)	Performance (at 1.23 V_{RHE})	Ref
Br-$BiVO_4$	100	2.23	This work
40-Ag-Pi/$BiVO_4$	100	2.32	[11]
BVO-NB-5P	100	1.47	[12]
Ni:$BiVO_4$	100	1.36	[13]
Au-doped $BiVO_4$	100	0.24	[14]
W (5%)-doped $BiVO_4$	100	0.61	[15]
Controlled nanostructured morphology of $BiVO_4$	100	1.98	[16]
S-BVO	100	1.80	[17]
F-BVO	100	0.28	[18]
oxygen vacancies BVO	100	2.00	[19]

Table S2 Impedance parameters obtained from EIS plots

Sample	R_s/Ω （Error/%）	R_{ct}/Ω （Error/%）	CPE/F （Error/%）
BVO	8.47 （0.89）	138.9 （2.40）	9.689E-5 （3.97）
Br-BVO	7.92 （1.02）	254.1 （3.13）	1.98E-4 （4.19）

References

[1] P. Luan, X. Zhang, Y. Zhang, Z. Li, U. Bach, J.J.C. Zhang, Dual Quantum Dot-Decorated Bismuth Vanadate Photoanodes for Highly Efficient Solar Water Oxidation, ChemSusChem, 12 (2019) 1240-1245.

[2] X. Huai, L. Girardi, R. Lu, S. Gao, Y. Zhao, Y. Ling, G.A. Rizzi, G. Granozzi, Z.J.N.E. Zhang, The mechanism of concentric $HfO_2/Co_3O_4/TiO_2$ nanotubes investigated by intensity modulated photocurrent spectroscopy (IMPS) and electrochemical impedance spectroscopy (EIS) for photoelectrochemical activity, Nano Energy, 65 (2019) 104020.

[3] G. Kresse, J.J.P.r.B. Furthmüller, Efficient iterative schemes for ab initio total-energy calculations using a plane-wave basis set, Phys. Rev. B, 54 (1996) 11169.

[4] J.P.J.P.R.L. Perdew, k. Burke, m. ernzerhof, 77 (1996) 3865.

[5] S.J.J.o.c.c. Grimme, Semiempirical GGA-type density functional constructed with a long-range dispersion correction, J Comput Chem., 27 (2006) 1787-1799.

[6] Y. Jia, L. Zhang, A. Du, G. Gao, J. Chen, X. Yan, C.L. Brown, X.J.A.m. Yao, Defect graphene as a trifunctional catalyst for electrochemical reactions, Adv. Mater., 28 (2016) 9532-9538.

[7] Á. Valdés, Z.W. Qu, G.J. Kroes, J. Rossmeisl, J.K. Nørskov, Oxidation and Photo-Oxidation of Water on TiO2 Surface, J. Phys. Chem. C, 112 (2008) 9872-9879.

[8] K.-H. Ye, Z. Wang, J. Gu, S. Xiao, Y. Yuan, Y. Zhu, Y. Zhang, W. Mai, S. Yang, Carbon quantum dots as a visible light sensitizer to significantly increase the solar water splitting performance of bismuth vanadate photoanodes, Energ. Environ. Sci., 10

(2017) 772-779.

[9] X. Shi, I.Y. Choi, K. Zhang, J. Kwon, D.Y. Kim, J.K. Lee, S.H. Oh, J.K. Kim, J.H. Park, Efficient photoelectrochemical hydrogen production from bismuth vanadate-decorated tungsten trioxide helix nanostructures, Nat. Commun., 5 (2014) 4775.

[10] L.J. Wang, J.Y. Bai, Y.J. Zhang, F. Mao, Y. Liu, H. Yuan, P.F. Liu, H.G. Yang, Controllable synthesis of conical $BiVO_4$ for photocatalytic water oxidation, J. Mater. Chem. A, 8 (2020) 2331-2335.

[11] Y. Gao, X. Li, J. Hu, W. Fan, F. Wang, D. Xu, J. Ding, H. Bai, W. Shi, Ag-Pi/$BiVO_4$ heterojunction with efficient interface carrier transport for photoelectrochemical water splitting, J Colloid Interf. Sci, 579 (2020) 619-627.

[12] K. Xue, H. Zhu, X. Zhao, L.A. Rodrigues, D.A. Reddy, Y. Zhang, L. Yu, Ni_3B modified $BiVO_4$ photoanodes for enhanced photoelectrochemical water splitting: The key role of Ni_3B on reducing the water oxidation barrier, Nano Res., 16 (2023) 12043-12049.

[13] S. Saxena, A. Verma, K. Asha, N.K. Biswas, A. Banerjee, V.R. Satsangi, R. Shrivastav, S. Dass, Nanostructured Ni:$BiVO_4$ photoanode in photoelectrochemical water splitting for hydrogen generation, Int. J Hydrogen Energ., 45 (2020) 26746-26757.

[14] C. Venkata Reddy, I. Neelakanta Reddy, K. Ravindranadh, K. Raghava Reddy, J. Shim, B. Cheolho, Au-doped $BiVO_4$ nanostructure-based photoanode with enhanced photoelectrochemical solar water splitting and electrochemical energy storage ability, Appl. Surf. Sci. , 545 (2021).

[15] L. Zhao, J. Wei, Y. Li, C. Han, L. Pan, Z. Liu, Photoelectrochemical performance of W-doped $BiVO_4$ photoanode, Journal of Materials Science: Materials in Electronics, J Mater Sci-Mater El., 30 (2019) 21425-21434.

[16] N.G. Deshpande, C.H. Ahn, R.R. Koli, A.S. Jamadar, D.S. Kim, Y.B. Kim, S.H. Jung, H.K. Cho, Controlled nanostructured morphology of $BiVO_4$ photoanodes for efficient on-demand catalysis in solar water-splitting and sustainable water-treatment, Appl. Surf. Sci., 514 (2020).

[17] M. Rohloff, B. Anke, O. Kasian, S. Zhang, M. Lerch, C. Scheu, A. Fischer, Enhanced Photoelectrochemical Water Oxidation Performance by Fluorine Incorporation in $BiVO_4$ and Mo:$BiVO_4$ Thin Film Photoanodes, ACS Appl. Mater. Interface, 11 (2019) 16430-16442.

[18] S. Wang, T. He, P. Chen, A. Du, K. Ostrikov, W. Huang, L. Wang, In Situ Formation of Oxygen Vacancies Achieving Near-Complete Charge Separation in Planar $BiVO_4$ Photoanodes, Adv. Mater., 32 (2020) 2001385.

[19] X. Yin, J. Li, L. Du, F. Zhan, K. Kawashima, W. Li, W. Qiu, Y. Liu, X. Yang, K. Wang, Y. Ning, C.B. Mullins, Boosting Photoelectrochemical Performance of $BiVO_4$ through Photoassisted Self-Reduction, ACS Appl. Energy Mater., 3 (2020) 4403-4410.